Optics Communications 410 (2018) 811–816

Contents lists available at ScienceDirect

Optics Communications

journal homepage: www.elsevier.com/locate/optcom

Isoplanatic patch of the human eye for arbitrary wavelengths

Guoqing Han [a,b], Zhaoliang Cao [a,*], Quanquan Mu [a,*], Yukun Wang [a,b], Dayu Li [a], Shaoxin Wang [a], Zihao Xu [a,b], Daosheng Wu [a,b], Lifa Hu [c], Li Xuan [a]

[a] State Key Laboratory of Applied Optics, Changchun Institute of Optics, Fine Mechanics and Physics, Chinese Academy of Sciences, Changchun, 130033, China
[b] University of Chinese Academy of Sciences, Beijing, 100049, China
[c] School of Science, Jiangnan University, Wuxi, 214122, China

ARTICLE INFO

Keywords:
Isoplanatic patch
Adaptive optics
Retinal imaging
Wave-front sensing
Ophthalmic optics

ABSTRACT

The isoplanatic patch of the human eye is a key parameter for the adaptive optics system (AOS) designed for retinal imaging. The field of view (FOV) usually sets to the same size as the isoplanatic patch to obtain high resolution images. However, it has only been measured at a specific wavelength. Here we investigate the wavelength dependence of this important parameter. An optical setup is initially designed and established in a laboratory to measure the isoplanatic patch at various wavelengths (655 nm, 730 nm and 808 nm). We established the Navarro wide-angle eye model in Zemax software to further validate our results, which suggested high consistency between the two. The isoplanatic patch as a function of wavelength was obtained within the range of visible to near-infrared, which can be expressed as: $\theta = 0.0028\lambda - 0.74$. This work is beneficial for the AOS design for retinal imaging.

1. Introduction

Adaptive optics (AO) has been extensively used in retinal imaging instruments, such as optical coherence tomography (OCT) and scanning laser ophthalmoscope (SLO), to improve image quality by correcting ocular aberrations. In 1997, Liang et al. [1] initially imaged the photoreceptors in the human eye using AO technology. Up to now several systems have obtained high-resolution images of cone and rod cells [2], nerve fibers [3], and retinal capillaries [4], which were used in visual research and early diagnosis of disease [5–8]. Similar to the AO used in astronomy, aberrations can be well corrected only in a small FOV for the retinal imaging system. The rays reflected from various retinal locations are propagated through the eye with different paths; thus, the produced aberrations differ for various FOVs. Nevertheless, a local region exists where the path differences are sufficiently small and the change of the ocular aberrations may be considered small enough that diffraction-limited resolution imaging can be almost achieved in this region, and it is called the isoplanatic patch [9]. For the outside region, the difference will observably increase, which causes a decline in imaging resolution. Ocular AO systems are therefore inherently limited in FOV, which is set in accord with the size of the isoplanatic patch generally.

In 1997, Liang et al. initially investigated the isoplanatic patch of the human eye, and the corrected results show that the quality of the retinal image has no obvious degradation at a wavelength of 633 nm within the FOV of 1° [1]. Maida et al. achieved the result that the isoplanatic patch ranges from 1°–2° by measuring the ocular aberrations for the wavelength of 830 nm [10]. In 2006, Tarrant et al. [11] and Atchison et al. [12] measured the isoplanatic patch with the result of 2° for the wavelength of 780 nm. In 2008, Bedggood and colleagues reported the isoplanatic patch to be approximately 0.8° at a 555 nm wavelength [13]. The same year Dubinin et al. [14] reported the angular size of the zone of constant wavefront aberrations varies from 1.5° to 2.5° for the wavelength of 780 nm. In 2012, Maciej Nowakowski and colleagues reported the patch size to be approximately 2° for the wavelength of 840 nm [15].

On the basis of the above research results, the isoplanatic patch is related to the wavelength, and this patch may be considered in two aspects: the diffraction-limited resolution of the optical system and the ocular transverse chromatism. Given that the former is proportional to the wavelength, a long wavelength indicates a large isoplanatic patch. Furthermore, the later affects the isoplanatic patch because it is related to wavelength. Hence, the relationship between the isoplanatic patch and wavelength is influenced by the above two aspects and cannot be directly calculated. Until today, the isoplanatic patch is obtained only at certain special wavelengths, and no universal formula is provided to compute it at an arbitrary wavelength. For retinal imaging, the

* Corresponding authors.
E-mail addresses: caozlok@ciomp.ac.cn (Z. Cao), muquanquan@ciomp.ac.cn (Q. Mu).

https://doi.org/10.1016/j.optcom.2017.11.055
Received 8 September 2017; Received in revised form 28 October 2017; Accepted 19 November 2017
Available online 29 November 2017
0030-4018/

Table 1
Geometry of the schematic wide-angle eye model.

Surface	Type	Conic constant	Radius (mm)	Thickness (mm)	Optical media
Ant cornea	Conic	−0.26	7.72	0.55	Cornea
Post cornea	Spherical	0	6.50	3.05	Aqueous
Pupil	Plane	0	Infinity	0	Aqueous
Ant ens	Conic	−3.1316	10.20	4.00	Lens
Post lens	Conic	−1	−6.00	16.3203	Vitreous
Retina	Spherical	–	−12	–	–

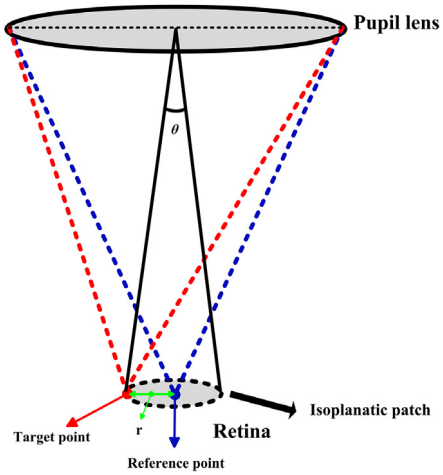

Fig. 1. Illustration of isoplanatic patch of a simplified eye.

wavelength of the imaging light is not fixed, for example, near-infrared light for photoreceptor imaging and visible light for capillaries imaging. The wavelength dependence of the isoplanatic patch means the size of the most suitable imaging FOV is different for different wavelengths, which might be of interest to retinal AO designers accordingly. Thus, in this study, the isoplanatic patch as a function of the wavelength is obtained at the visible–near-infrared waveband by measuring on-axis and off-axis aberrations of different living eyes at various wavelengths (655 nm, 730 nm and 808 nm) and eye model simulation.

2. Method

2.1. Measurements

The structure of the eye may be simplified as the combination of a pupil lens and retina, as shown in Fig. 1. The reflected light from the reference and target points goes through different paths; thus, the distorted wavefront differs as well. If the difference is sufficiently small and has almost no effect on image resolution, the isoplanatic patch should be the circular area with the radius of r and its corresponding FOV is θ. The Maréchal criterion [16] is typically used to define the aberration difference between the reference and target points, and the root mean square (RMS) of the difference should be less than $\lambda/14$ (λ is the relevant wavelength). To calculate the RMS of the wavefront difference conveniently, the wavefront is expressed using up to and including 7th-order Zernike polynomials (OSA standard) [17]. Tips and tilts were not taken into account as they do not affect the resolution. Having defined the boundary limit of RMS wavefront error, the isoplanatic region was obtained by subtracting the reference wavefront coefficients from wavefronts coefficients for each field angle θ, the reference position is the central fovea of retina.

An optical setup is designed to measure the isoplanatic patch of the human eye, as shown in Fig. 2. A laser is used as the light source, and its coherence is decreased by a diffuser. The light is coupled with fiber with lens 1 (L1) and then collimated by L2. The collimated beam is expanded out by L3 and L5 to match the aperture of the pupil. An annular aperture is utilized to eliminate the reflected light from the cornea. The zoomed light is reflected by the beam splitter 2 (BS2) and then focused on the retina. The reflected light, which comes from the retina, passes through L7 and L8 and is then detected by a Shack–Hartmann wavefront sensor (S–H WFS). The S–H WFS had a lenslet array of 20×20, 3 mm diameter, and 515 Hz acquisition frequency. The focus length of the lenslet array is 3.2 mm and the subaperture diameter is 150 μm. A pupil camera is used to track the axial and vertical position of the pupil in order to check that it is in the conjugate position with S–H WFS from beginning to the end. A fixation target is utilized to control the focused position of the incident beam at the retina. It is composed of seven rectilinear light sources, which will be on and off alternately. The incident beam is focused on various retinal positions by staring at the fixation target. Three measurements are taken every position and the average of them is the aberration of that position. In the experiment, the off-axis aberrations from −1.5° to 1.5° relative to central fovea with a step of 0.5° in the horizontal direction were acquired.

Table 2
Refractive indices for the wavelengths used in computations.

Medium	458 nm	543 nm	589.3 nm	632.8 nm
Cornea	1.3828	1.3777	1.376	1.3747
Aqueous	1.3445	1.3391	1.3374	1.336
Lens	1.4292	1.4222	1.42	1.4183
Vitreous	1.3428	1.3377	1.336	1.3347

The measurement data came from the left eyes of four healthy people (three male and one female). Spherical errors ranged between −0.5 D and −7 D (−3.60 ± 2.63 D). The measured wavefront is expressed with the first 7th-order Zernike polynomials across a pupil diameter of 6.0 mm. Accommodation was not paralyzed for the experiment as all the pupil diameters were over 6.0 mm in darkroom condition. Eye aberrations of the examined subjects are measured for the wavelengths of 655 nm, 730 nm, and 808 nm and the calculated results are shown in Fig. 3. The dashed line represents the Maréchal criterion, and the real line is the fitting curve of the measured data. The further results indicate that the mean values of the isoplanatic patch are 0.95 ± 0.15°, 1.16 ± 0.13°, and 1.37 ± 0.14° respectively.

2.2. Eye model simulation

To compare with the experimental results and get the isoplanatic patch as a function of wavelength, the Navarro wide-angle eye model [18,19] was chosen, which reproduce off-axis aberrations and chromatic aberrations based on anatomical and experimental data. It consists of two spherical and three aspheric surfaces and is considered as one of the most close to the real human eye in ophthalmology. The schematic eye is depicted in Fig. 4, Tables 1 and 2 present the geometrical parameters and the refractive indices, respectively. For λ = 543 nm, the focal length of this schematic eye is 22.03 mm in the image space (the effective focal length in air is 16.47 mm), and the refractive power is 60.7 D. The pupil size was set to 6.0 mm.

We collected the aberration data from 11 field points in 0.5 deg increments in horizontal direction, since the eye model is centrally symmetric with respect to the optical axis. Fig. 5 shows RMS of the wavefront difference of different wavelength for the eye model. The

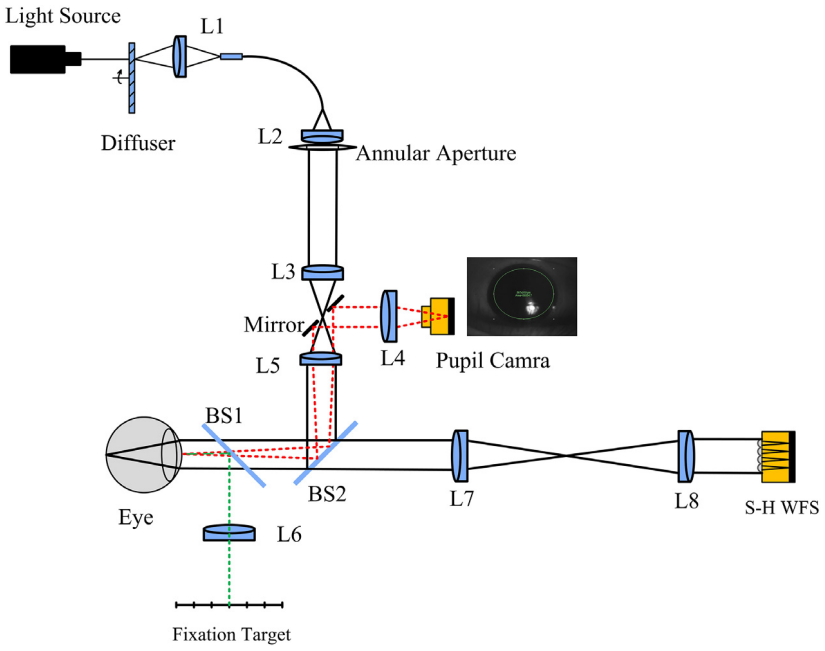

Fig. 2. Optical layout for the isoplanatic patch measurement.

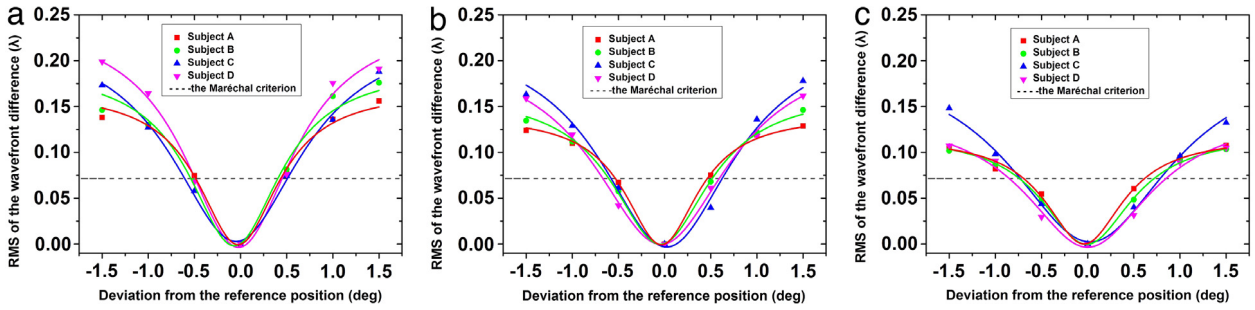

Fig. 3. RMS of the wavefront difference of the four subjects: (a) 655 nm; (b) 730 nm; (c) 808 nm. The reference position is the central fovea.

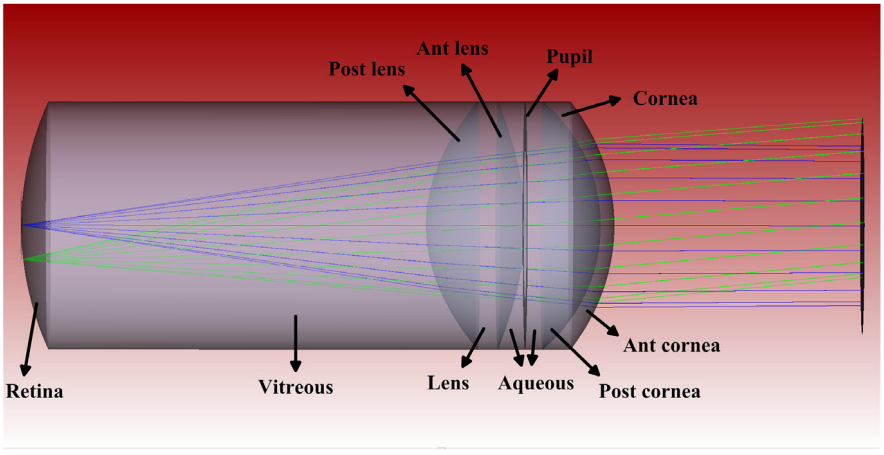

Fig. 4. The Navarro wide-angle eye model.

differences become larger as the distance from the reference position increases. The dashed line represents the Maréchal criterion, and the real line is the fitting curve of the measured data. The wavelength ranges from 400 nm to 900 nm at intervals of 100 nm and the simulated results show that isoplanatic patch are 0.34°, 0.68°, 1°, 1.28°, 1.52°, 1.76° respectively.

3. Results and discussion

The on-axis and off-axis aberrations were measured according to the method described in Section 2.1. Fig. 6 shows the Zernike coefficients with the bigger change for the wavelength of 808 nm. It indicates that the variation of the aberrations is mainly influenced by defocus and

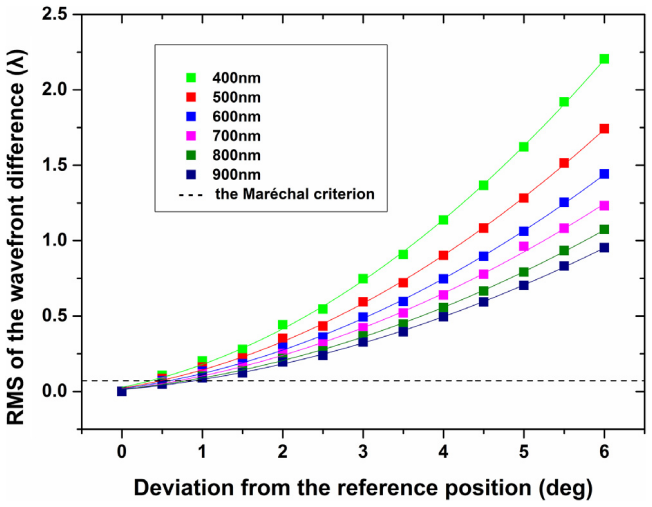

Fig. 5. RMS of the wavefront difference of different wavelength for the eye model.

astigmatism. The Zernike coefficients of the two (Z4 & Z5) show positive growth with eccentricity for all subjects. Besides, coma (Z8) may have an effect on the isoplanatic patch, which shows negative growth with eccentricity for subject A and subject D, and no obvious change for subject B and subject C. The mean experimental values of four living eye are 0.95 ± 0.15°, 1.16 ± 0.13°, and 1.37 ± 0.14° respectively for the wavelength of 655 nm, 730 nm and 808 nm.

For eye model, the isoplanatic patch ranges from 0.34° to 1.76° in the visible–near-infrared band, which exhibits a trend of approximately linear growth with respect to the wavelength. A linear fit to the data is obtained:

$$\theta = 0.0027\lambda - 0.85 \quad (1)$$

Where the unit of wavelength is nanometer, as is shown in Fig. 7, the black square and the solid line represents simulation results and Eq. (1), respectively. The contrast results of the two reflects that the experimental values are all quite close to Eq. (1). Therefore, we fitted the experimental data linearly, as shown as follows:

$$\theta = 0.0028\lambda - 0.74 \quad (2)$$

The red dot and solid line was the experimental discrete data and the Eq. (2), respectively. According to Eqs. (1) and (2), it can be seen that the growth trend of the two is approximately the same and there is a consistent difference (0.11 deg) between the two. In our opinion, it is possibly caused by three reasons: (1) the model error: the agreement between aberrations of the Navarro wide-angle eye model and average experimental data is quite reasonable in general. However, on-axis coma value of simulation is larger than the experimental value, leading to potentially smaller RMS of the wavefront difference and larger value of the isoplanatic patch size; (2) the difference of statistical subjects: the eye model is based on anatomical and experimental data, which are from lots of eyes. Nevertheless, our aberration data are just from four volunteers, which may be one of the reasons for the error; (3) the difference of aberrations: the aberrations of the eye model are stationary, whereas the aberrations of real eye are dynamic. Suggestions have been made that the changes in ocular aberrations could be due to eye movements, retinal pulsation, microfluctuations of the lens and variations in the tear film layer [20–22]. We can only try to weaken the influence of these factors to the measurement by means of a fixation target, carefully pupil location, eye sufficient rest and repeated measurements of each position, but cannot completely rule them out.

To further validate the results above, previous studies are added in Fig. 7, in which Atchison et al. study and Bedggood et al. study are

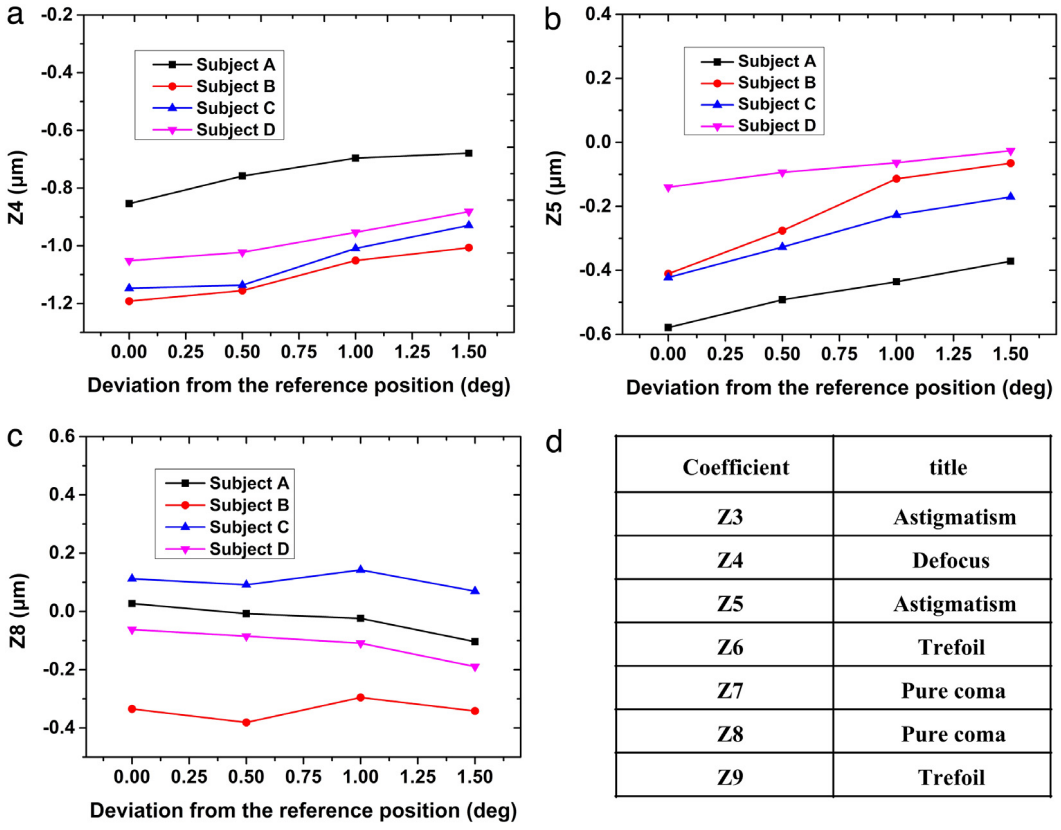

Coefficient	title
Z3	Astigmatism
Z4	Defocus
Z5	Astigmatism
Z6	Trefoil
Z7	Pure coma
Z8	Pure coma
Z9	Trefoil

Fig. 6. Zernike coefficients for different positions for the wavelength of 808 nm.

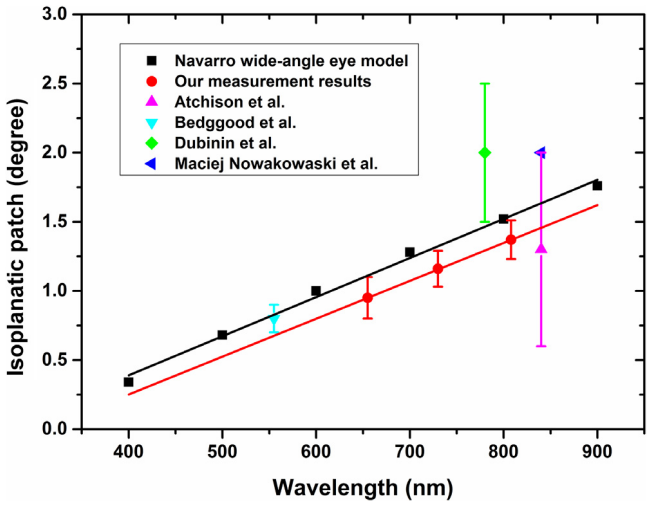

Fig. 7. The isoplanatic patch size under the condition of different wavelengths. (For interpretation of the references to color in this figure legend, the reader is referred to the web version of this article.)

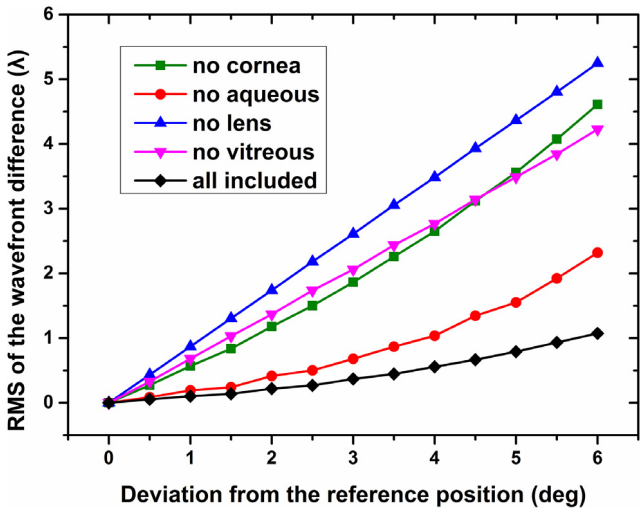

Fig. 8. RMS of the wavefront difference for the wavelength of 800 nm.

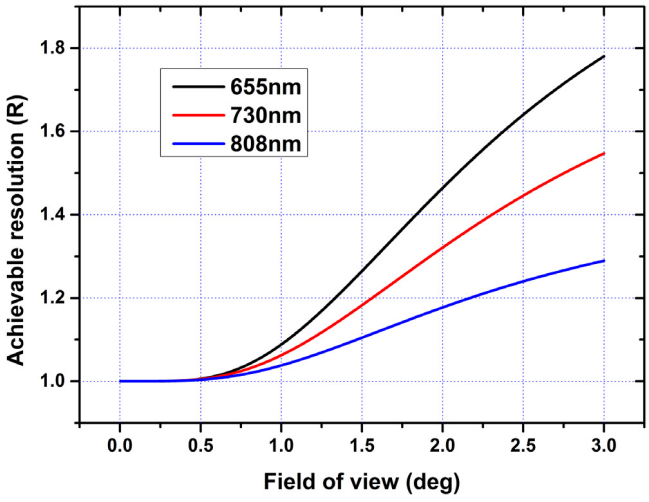

Fig. 9. The achievable resolution of different FOV.

quite close to the value obtained from eye model and measurement experiments. Dubinin et al. study used a more relaxed criterion than the Maréchal, being a residual wavefront mean square error of 1 rad^2. This corresponds to a Strehl ratio of 0.37. The Maréchal, on the other hand, corresponds to a Strehl ratio of 0.8. In addition, smaller pupil sizes were used, resulting in aberrations of lower magnitude. It therefore provide a larger estimate of patch size. Maciej Nowakowski et al. study also overestimated the patch size due to the use of the same relaxed criterion. All analyses illustrate that Eq. (2) maybe appropriate to describe the relationship between the isoplanatic patch and wavelength.

The Navarro wide-angle eye model consists of two spherical and three aspheric surfaces, which contains four types of optical media (cornea, aqueous, lens and vitreous). To investigate which component of the model is the main contributor to isoplanatism, we removed each optical media from the eye model in turn and recalculated the RMS of the wavefront difference for the wavelength of 800 nm (see Fig. 8). After cornea, aqueous, lens and vitreous were removed, the corresponding isoplanatic patches are 0.2°, 0.27°, 0.2° and 0.64°, whereas it is 1.56° when all optical media included. It indicates that cornea, lens and vitreous have a major influence on the isoplanatic patch of human eye and aqueous has a relatively small impact.

As is well known, the imaging resolution depends both upon the diffraction limit and aberration of the optical imaging system. The former is related to wavelength and numerical aperture (NA) of system, which is a fixed value when wavelength and NA are determined. Therefore, the achievable imaging resolution of the system will be directly affected by the magnitude of residual aberration after correction in ocular AO system. It is fairly accepted that the resolution is almost unaffected within the isoplanatic patch owing to small enough residual aberration ($<\lambda/14$). However, the residual aberration will become greater with increasing distance from the reference point on the retina (Figs. 3 and 5), which results in a decrease in imaging resolution. The achievable resolution can be expressed approximately as the function of the Strehl ratio [23] as

$$R_a = 1.22\frac{\lambda}{D\sqrt{S}} \cdot f = \frac{1}{\sqrt{S}} \cdot R, \tag{3}$$

where λ is the wavelength, D is the aperture of eye pupil, f is focal length of eye, S is the Strehl ratio and R represents the diffraction-limited resolution. According to Eq. (3) and the aberration data from Fig. 3, the achievable resolution in different FOV are shown in Fig. 9. The results indicate that the achievable resolution will drop to 1.5 times the diffraction limit for the FOV of 2° and 1.8 times the diffraction limit for the FOV of 3° when the wavelength is 655 nm. For the wavelength of 730 nm, they are 1.3 and 1.6 times respectively. For the wavelength of 808 nm, they are 1.2 and 1.3 times respectively. The shorter the wavelength, the faster the resolution drops. In ocular AO system, it is an inverse relation between FOV and the achievable resolution according to Fig. 9, which is the reason that the FOV is usually set to the same size as the isoplanatic patch to get the highest resolution. However, the FOV may be properly expanded in accordance with the conclusion (Fig. 9) to obtain images with larger views when the requirements for imaging resolution are relaxed.

4. Conclusions

In this paper, the isoplanatic patch of the human eye is investigated for an arbitrary wavelength. An optical setup is initially designed and established in the laboratory and the eyes of the four subjects are then measured for the wavelengths of 655, 730, and 808 nm. The mean value of isoplanatic angle was about 0.95 ± 0.15°, 1.16 ± 0.13°, and 1.37 ± 0.14° respectively. It exhibits a trend of linear growth with respect to the wavelength, which is approximately consistent with the simulation result of the Navarro wide-angle eye model and can be expressed as: $\theta = 0.0028\lambda - 0.74$,within the range of visible to near-infrared. Furthermore, previous results of other researchers are found

to be quite close to our results. The achievable resolution declines as the field of view increases and the shorter the wavelength, the faster the resolution drops. The achievable resolution will drop to 1.5, 1.3 and 1.2 times the diffraction limit respectively for the wavelength of 655 nm, 730 nm and 808 nm when the FOV is 2°. For the FOV of 3°, they are 1.8, 1.6 and 1.3 times the diffraction limit.

Acknowledgment

This work is supported by the National Natural Science Foundation of China with grant numbers 61205021 and 11204299.

References

[1] J. Liang, D.R. Williams, D.T. Miller, Supernormal vision and high-resolution retinal imaging through adaptive optics, J. Opt. Soc. Am. A 14 (1997) 2884.
[2] A. Roorda, D.R. Williams, The arrangement of the three cone classes in the living human eye, Nature 397 (1999) 520.
[3] A. Roorda, F. Romero-Borja, I.I.I.W. Donnelly, H. Queener, T. Hebert, M. Campbell, Adaptive optics scanning laser ophthalmoscopy, Opt. Express 10 (2002) 405.
[4] N. Ling, Y. Zhang, X. Rao, C. Wang, Y. Hu, W. Jiang, High resolution mosaic image of capillaries in human retina by adaptive optics, Chin. Opt. Lett. 3 (2005) 225.
[5] E.A.E. Phan A D T, T.Y. Chui, In vivo microvascular changes in diabetic patients without clinically severe diabetic retinopathy, 5 (2012).
[6] M.J. Booth, Adaptive optical microscopy: The ongoing quest for a perfect image, Light Sci. Appl. 3 (2014) e165.
[7] S. Zayit-Soudry, J.L. Duncan, R. Syed, M. Menghini, A.J. Roorda, Cone structure imaged with adaptive optics scanning laser ophthalmoscopy in eyes with nonneovascular age-related macular degeneration, in: Investigative Ophthalmology & Visual Science, 2013, p. 7498.
[8] G. Querques, C. Kamami-Levy, A. Georges, A. Pedinielli, E.H. Souied, Appearance of regressing drusen on adaptive optics in age-related macular degeneration, Ophthalmology 121 (2014) 611.
[9] C.M.D. Michael Bass, Jay Enoch, Guifang Li, Vasudevan Lakshminarayanan, Carolyn MacDonald, Virendra N. Mahajan, Eric Van Stryland, Handbook of Optics, third ed., McGraw-Hill Education, 2009, p. 553.
[10] E.M. Maida, K. Venkateswaran, J. Marsack, A. Roorda, What is the Size of the Isoplanatic Patch in the Human Eye? 1999.
[11] J. Tarrant, A. Roorda, The extent of the isoplanatic patch of the human eye, Arvo Meet. Abstr. 47 (2006).
[12] D.A. Atchison, S.D. Lucas, R. Ashman, M.A. Huynh, D.W. Schilt, P.Q. Ngo, Refraction and aberration across the horizontal central 10° of the visual field, Optom. Vis. Sci. 83 (2006) 213.
[13] P. Bedggood, M. Daaboul, R. Ashman, G. Smith, A. Metha, Characteristics of the human isoplanatic patch and implications for adaptive optics retinal imaging, J. Biomed. Opt. 13 (2008) 024008.
[14] A.V. Dubinin, T.Y. Cherezova, A.I. Belyakov, A.V. Kudryashov, Isoplanatism of the optical system of the human eye, J. Opt. Technol. 75 (2008) 172.
[15] M. Nowakowski, M. Sheehan, D. Neal, A.V. Goncharov, Investigation of the isoplanatic patch and wavefront aberration along the pupillary axis compared to the line of sight in the eye, Biomed. Opt. Express 3 (2012) 240.
[16] E.W.M. Born, Principles of Optics, fifth ed., Pergamon Press, 1970.
[17] L.N. Thibos, R.A. Applegate, J.T. Schwiegerling, R. Webb, Standards for reporting the optical aberrations of eyes, J. Refractive Surg. 18 (2002) S652, Thorofare, N.J. : 1995, V.S.T.M.V. science, a. its.
[18] I. Escudero-Sanz, R. Navarro, Off-axis aberrations of a wide-angle schematic eye model, J. Opt. Soc. Am. A 16 (1999) 1881.
[19] R. Navarro, J. Santamaría, J. Bescós, Accommodation-dependent model of the human eye with aspherics, J. Opt. Soc. Am. A 2 (1985) 1273.
[20] S. Gruppetta, F. Lacombe, P. Puget, Study of the dynamic aberrations of the human tear film, Opt. Express 13 (2005) 7631.
[21] H. Hofer, P. Artal, B. Singer, J.L. Aragón, D.R. Williams, Dynamics of the eye's wave aberration, J. Opt. Soc. Am. A 18 (2001) 497.
[22] K.M. Hampson, C. Dainty, I. Munro, C. Paterson, Weak correlation between the aberration dynamics of the human eye and the cardiopulmonary system, J. Opt. Soc. Am. A 22 (2005) 1241.
[23] D.W. Tyler, A.E. Prochko, Adaptive optics design for the advanced electro-optical system (AEOS), in: Final Report 32, 1994.